First-principles studies of chromium line-ordered alloys in a molybdenum disulfide monolayer

N.F. Andriambelaza[a,*], R.E. Mapasha[a], N. Chetty[a,b]

[a]Department of Physics, University of Pretoria, Pretoria 0002, South Africa
[b]National Institute for Theoretical Physics, Johannesburg, 2000, South Africa

Abstract

Density functional theory calculations have been performed to study the thermodynamic stability, structural and electronic properties of various chromium (Cr) line-ordered alloy configurations in a molybdenum disulfide (MoS_2) hexagonal monolayer for band gap engineering. Only the molybdenum (Mo) sites were substituted at each concentration in this study. For comparison purposes, different Cr line-ordered alloy and random alloy configurations were studied and the most thermodynamically stable ones at each concentration were identified. The configurations formed by the nearest neighbor pair of Cr atoms are energetically most favorable. The line-ordered alloys are constantly lower in formation energy than the random alloys at each concentration. An increase in Cr concentration reduces the lattice constant of the MoS_2 system following the Vegard's law. From density of states analysis, we found that the MoS_2 band gap is tunable by both the Cr line-ordered alloys and random alloys with the same magnitudes. The reduction of the band gap is mainly due to the hybridization of the Cr 3*d* and Mo 4*d* orbitals at the vicinity of the band edges. The band gap engineering and magnitudes (1.65 eV to 0.86 eV) suggest that the Cr alloys in a MoS_2 monolayer are good candidates for nanotechnology devices.

Keywords: two dimensional material, molybdenum disulfide, density functional theory, alloys.

1. Introduction

In the last few years, two dimensional (2D) layered materials have become an important area of research in material science. Due to their reduced dimensionality, they possess unique electronic and optical properties different from their bulk counterparts [1, 2, 3, 4]. These fascinating properties make 2D materials suitable candidates for various applications in nanoelectronic technologies [2, 4, 5]. The successful synthesis of graphene [6] was the starting point for the extensive exploration of different types of 2D materials. Graphene has extremely high charge carrier mobility and exceptional mechanical flexibility [1, 4]. However, it is a zero band gap material [1]. Consequently, this limits the direct application of graphene in the nanotechnological devices. Many experimental and theoretical efforts have been made to open a band gap in a graphene system [7, 8, 9, 10, 11]. A sizable band gap was achieved, but it was found to be either too small [7, 8, 9] or too large [10, 11]. This issue drove researchers to explore other 2D materials such as boronitrene (h-BN) [12] and transition metal dichalcogenides (TMD) [13]. Some of the TMD 2D systems are particularly interesting due to their tremendous properties such as high mechanical strength, direct band gap and optical transparency [14, 15, 16, 17]. Because of these exotic properties, TMD materials are suitable for applications in the nanoelectronic and optoelectronic devices [15, 18, 19].

TMD materials have the chemical formula MX_2, where M is a transition metal element and X stands for chalcogen from group VIB element. Depending on the type of the transition element and the chalcogen, TMD 2D systems can be an insu-

*Corresponding author
Email address: arinala.f@gmail.com (N.F. Andriambelaza)

lator (e.g. Zirconium disulfide (ZrS_2)), metal (e.g. Niobium disulfide (NbS_2)), semimetal (e.g. Tungsten telluride (WTe_2)) and semiconductor (e.g. Chromium disulfide (CrS_2), Molybdenum disulfide (MoS_2) and Tungsten disulfide (WS_2)) [20]. Amongst the various TMD monolayers, MoS_2 monolayer is the most widely studied material owing to some of its special semiconducting properties similar to those of carbon-based graphene [21, 22]. As in other semiconductors, the electronic and optical properties of MoS_2 2D material are usually controllable by tuning the band gap. Thus, engineering the band gap of MoS_2 monolayer is important for designing nanoelectronic devices.

Historically, alloying has been used as an effective method to tune electronic structures of 3D semiconductor materials [23, 24, 25]. Recently, several experimental and theoretical studies have investigated the formation possibilities and electronic properties of alloys in the 2D TMD materials [26, 27, 28, 29]. For instance, Xu *et al.* [26] reported a chemical vapor deposition (CVD) strategy for the growth of $Mo_{1-x}W_xS_2$ and $MoS_{1-x}Se_x$ monolayers. It was found that W (Se) alloys increase (reduce) the band gap of pristine MoS_2 monolayer from 1.83 eV to 1.97 eV (1.55 eV). It was suggested that this band gap engineering is important to further optimize the performance of nanoscale photoelectronic devices. Tongay *et al.* [29] successfully synthesized $Mo_{1-x}W_xSe_2$ and reported that the band gap of a MoS_2 monolayer can be tuned by varying the W concentration. Using density functional theory (DFT) approach, Xi *et al.* [27] reported that the band gap of MoS_2 monolayer is tunable by W alloying and its enthalpy of formation is exothermic. Komsa *et al.* [28] investigated the thermodynamic stability and electronic properties of random $Mo_{1-x}W_xS_2$, $MoS_{1-x}Se_x$, $MoS_{1-x}Te_x$ and $MoSe_{1-x}Te_x$ alloys using DFT. They found that the formation energies for $MoS_{1-x}Te_x$ and $MoSe_{1-x}Te_x$ alloys are positive although very small and for $Mo_{1-x}W_xS_2$ and $MoS_{1-x}Se_x$ are negative. They also noted that the chalcogen alloys usually reduce the band gap of a MoS_2 monolayer, whereas W alloys raise it during the increase in concentration. In general, Se, Te and W alloys in a MoS_2 monolayer are exothermic and fine tune the band gap. This band gap engineering in a MoS_2 system is essential for the fabrication of nanoelectronic devices. Chromium (Cr) is in the same periodic table group with Mo and W, and thus deserve to be investigated as well. Xie [30] reported that creating TMD alloys within the same transition metal group is usually feasible. This has been noted in the case of W replacing Mo or Se and Te replacing S in a MoS_2 monolayer. These type of systems have a very small lattice mismatch with the MoS_2 monolayer. To the best of our knowledge, there is no detailed publications on the study of $Mo_{1-x}Cr_xS_2$ and the transition from MoS_2 to CrS_2 monolayer through Cr alloying.

Studying all the possible configurations of alloys in a MoS_2 monolayer using a DFT method is not a tractable task. Alloys in a 2D materials can appear in different configurations such as clusters (many shapes : triangle-like, square, circular, etc), lines and can randomly scattered away from each other in different forms. The number of possible distinct configurations at any concentration with a number n of the Cr atoms is obtained by :

$$\frac{N!}{n!(N-n)!}\,, \tag{1}$$

where N is the total number of Mo sites in a monolayer. For instance, in the case of 20% concentration constituted by a total of 5 Cr atoms replacing the Mo atoms in a 5×5 supercell, there are 53130 possible configurations. Computing all of these possible configurations is practically impossible as this requires huge computational resources. To reduce this difficulty, adopting typical configurations is helpful. Experimentally, it was reported that the TMD alloys are usually synthesized in random phases at high temperatures [30]. However, DFT studies at 0 Kelvin have reported that ordered phases have a lower formation energy than random phases [30, 31, 32]. Most of the previous studies on TMD alloys considered various cluster configurations using a DFT approach [30, 31, 33]. A line alloy which is another form of ordered alloy can appear in different configurations in a MoS_2 monolayer, therefore worth to be studied and to know the most energetically favorable configuration. Komsa *et al.* [34] have studied line-ordered alloys of the

Se atoms substituting the S atoms in a MoS_2 monolayer. They stated that line-ordered alloy can be a way to alter the electronic properties of MoS_2 monolayer. The knowledge of the transition metal line-ordered alloys substituting the Mo sites is scarce.

In this paper, we present a comparative study of the physical properties of line-ordered alloys and random alloys of Cr atoms in a MoS_2 monolayer using a DFT approach. In a MoS_2 monolayer supercell, the possible line-ordered alloy configurations are few and can easily be identified at each Cr concentration. However, for the random alloys, a large number of different configurations are possible. Special quasi-random structure (SQS) method [35] is a tool that can mimic the possible random alloy configurations at each concentration. This method has been successfully applied to various alloys in a MoS_2 monolayer [33].

Based on the alloy formation energy analysis, we identify the lowest energy configurations for line-ordered alloys as well as random alloys at each concentration, when the Cr atoms substitute the Mo atoms. To have an insight to the electronic properties of the lowest energy configurations, the densities of states (DOS) were plotted. As opposed to W alloys, the band gap of $Mo_{1-x}Cr_xS_2$ decreases with the increase in Cr concentration. The band gap of MoS_2 monolayer is finite but tunable, making it a good candidate in nanoelectronic devices.

2. Methodology

We have systematically investigated the thermodynamic stability, the structural and electronic properties of $Mo_{1-x}Cr_xS_2$ alloys using the DFT method implemented in the Vienna *ab-initio* simulation package (VASP) [36, 37]. To describe the core electron interactions, projector augmented wave (PAW) pseudopotential [38] were used. The generalized gradient approximation (GGA) exchange correlation parameterized by Perdew, Burke, and Ernzerhof (PBE) [39] was employed to treat the exchange correlation interactions. The supercell size, kinetic energy cut-off and Brillouin zone sampling convergence tests were conducted, and a 5×5 supercell was chosen. A kinetic energy cutoff of 300 eV for the plane wave expansion and $2 \times 2 \times 1$ k-point mesh were used. All the structures were fully relaxed. The convergence threshold was 10^{-5} eV for energies and 2×10^{-2} eV/Å for forces. To suppress interactions between adjacent supercells, a vacuum spacing of 15 Å was constructed in the perpendicular direction.

To examine the relative stability of the distinct possible configurations of $Mo_{1-x}Cr_xS_2$ alloys, the formation energy of each configuration was evaluated. The formation energy (E_{form}) is given by:

$$E_{form} = E_{Mo_{1-x}Cr_xS_2} - (1-x)E_{MoS_2} - xE_{CrS_2}\ , \qquad (2)$$

where $E_{Mo_{1-x}Cr_xS_2}$, E_{MoS_2} and E_{CrS_2} are the total energies of the mixed compound, the pristine MoS_2 and the pristine CrS_2 monolayers, respectively. The x parameter is the concentration of Cr introduced in a MoS_2 monolayer [40].

The different flavors of GGA functional [39, 41, 42, 43, 44] are known to underestimate the energy band gap of a material. In order to improve our band gap values, the hybrid functional of Heyd, Scuseria, and Ernzerhof (HSE06) [45] was also used. At the end of our discussion, we briefly compare the band gap values obtained from GGA functional with those obtained from the HSE functional.

The Cr substitution alloys in a MoS_2 monolayer ($Mo_{1-x}Cr_xS_2$) can be generalized as a binary $A_{1-x}B_x$ alloy. For a perfect random alloy, the correlation function is given by $\prod_{k,m}(R) = (2x-1)^k$, where $k = 2, 3, ...$ indicates the pair (2), triple (3),... correlation functions; $m = 1, 2, 3, ...$ indicates the first, second and third,...,nearest-neighbor distances and x represent the concentration of the substituted atoms [46]. In the SQS method, the sites i occupied by atoms A or B are assigned to a variable σ_i equals to -1 or 1, respectively. The correlation function for this binary alloy can be written as $\prod_{k,m} = \frac{1}{N_{k,m}} \sum_{\{k,m\}} \sigma_1\sigma_2...\sigma_k$, where $N_{k,m}$ is the total number of shape that can be obtained when varying k and m. In the present study, only the nearest-neighbor pairs are scrutinized, since the interactions between far distant neighbors have been reported not to have much effect on the total energy [33]. In this model (nearest neighbor pair), the correlation function

$\Pi_{2,1}$ is given by $\Pi_{2,1} = \frac{1}{N_{bond}} \sum_{j,h=1,N}^{j>h} \sigma_j \sigma_h$, where N_{bond} is the number of bonds between nearest neighbor metals, N is the total number of transition metal in the supercell, j and h represent the two pair sites considered. If the total number of the nearest-neighbor bonds between $A-A$ (Mo-Mo), $B-B$ (Cr-Cr) and $A-B$ (Mo-Cr) atoms are denoted by N_{AA}, N_{BB} and N_{AB}, respectively, the correlation function can be written as :

$$\Pi_{2,1} = \frac{N_{AA} + N_{BB} - N_{AB}}{N_{AA} + N_{BB} + N_{AB}}. \tag{3}$$

The number of atoms A (Mo) and B (Cr) in an $A_{1-x}B_x$ alloy is given by: $N_A = N(1-x)$ and $N_B = Nx$. In addition, assuming that z is the coordination number of atoms in the system, N_A and N_B are related to the number of bonds as:

$$\begin{cases} N_A = \frac{N_{AB}+2N_{AA}}{z} \\ N_B = \frac{N_{AB}+2N_{BB}}{z} \end{cases} \tag{4}$$

Therefore, the correlation function in equation. 3 becomes :

$$\Pi_{2,1} = 1 - 4x + \frac{8N_{BB}}{Nz}. \tag{5}$$

Thus, equation. 5 shows that the correlation function can be completely described by N_{BB}. The SQS configurations are considered to have the same correlation functions as the perfect random alloys: $\prod_{2,1}(R) = \prod_{2,1}(SQS)$ [46]. Using this equality and equation. 5, we found that the number of $N_{BB} = \frac{1}{2}x^2Nz$ in a TMD monolayer. In our study, $N = 25$ and $z = 6$ in a 5×5 supercell of MoS_2 monolayer. It can be shown that at $x = 0.2, 0.4, 0.6$ and 0.8 the $N_{BB} = 3, 12, 27$ and 48 respectively, yielding the SQS random alloy configurations. Many random alloys configurations are possible but the optimum SQS configurations are those that have the same correlation function as the perfect random alloy, i.e, pair, triple, etc.

3. Results and discussion

In order to study the effect of the Cr substitutional dopants on the thermodynamic stability, structural and electronic properties of a MoS_2 monolayer, the physical properties of the pristine MoS_2 and CrS_2 monolayers need to be understood first. In this section, we investigate the structural and electronic properties of these pristine systems. Thereafter, the Cr atoms are introduced into a MoS_2 monolayer by occupying the Mo sites only. An incorporation of the Cr atoms into a MoS_2 monolayer is treated in two cases; firstly, the low Cr concentration has been considered and secondly, the high concentration has been taken into account to form the alloys.

3.1. Pristine MoS_2 and CrS_2 monolayers

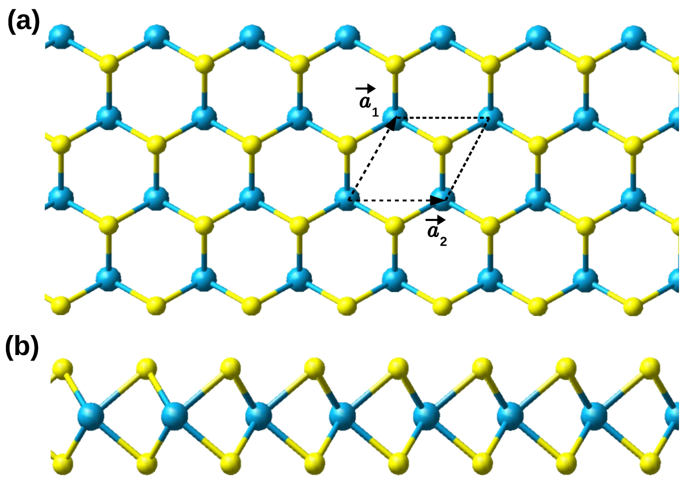

Figure 1: (a) Top view and (b) side view of the 2D TMD MoS_2 or CrS_2. The blue spheres indicate the transition metal atoms and the light yellow spheres indicate the sulfur (S) atoms. $\vec{a_1}$ and $\vec{a_2}$ are the lattice vectors. A unit cell is drawn with dashed lines.

The 2D TMD (MoS_2 and CrS_2) have different polymorphs such as the hexagonal and tetragonal [47]. Previous studies reported that the hexagonal structures of MoS_2 and CrS_2 monolayers are the most stable ones [20]. Top view and side view of the hexagonal TMD monolayer are shown in figure. 1. The transition metal (Mo or Cr) layer is sandwiched between the two adjacent sulfur (S) layers and form covalent bonds. The transition metal atoms occupy one sublattice of the hexagon and the S atoms occupy the other.

The fully optimized lattice constant for the MoS_2 and CrS_2 monolayers are found to be 3.18 Å and 3.05 Å, respectively. The bond lengths Mo-S and Cr-S are 2.41 Å and 2.29 Å, re-

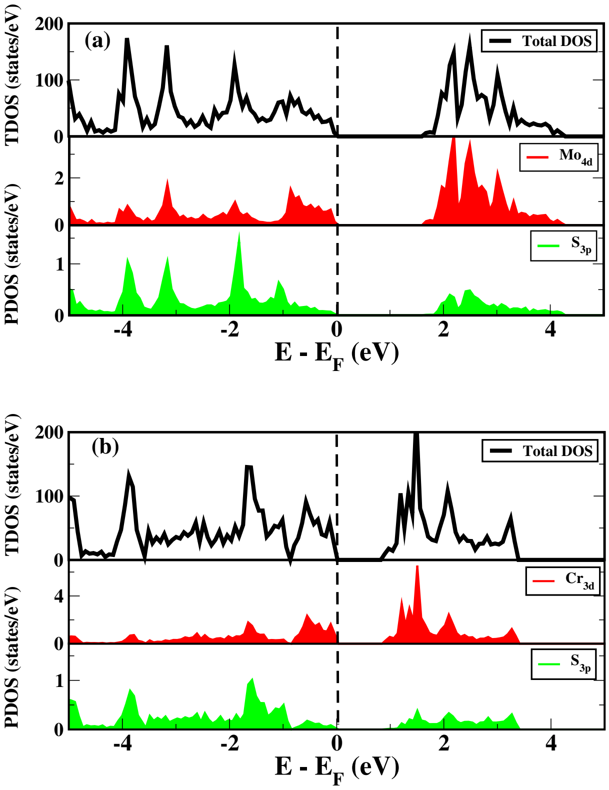

Figure 2: The total density of states (TDOS) for the pristine (a) MoS_2 and (b) CrS_2 monolayers (black lines). The red and green curves are the projected density of states (PDOS) for the transition metal *d* orbitals and S 3*p* orbitals, respectively. The dashed vertical lines indicate the Fermi level.

spectively. These values agree quite well with the experimental and the previous DFT data [48, 49, 50].

To study the electronic properties of the pristine MoS_2 and CrS_2 monolayers, density of states (DOS) were evaluated. Figure. 2 shows the total DOS (TDOS) for pristine MoS_2 (figure. 2(a)) and CrS_2 (figure. 2(b)) monolayers. These plots present a gap between the top of the valence band (VBM) and the bottom of the conduction band (CBM) indicating that both the pristine systems are semiconductors. We found that the band gaps of MoS_2 and CrS_2 monolayers are 1.65 eV and 0.86 eV, respectively. These values are consistent with the previous theoretical and experimental data shown in Table. 1. The PDOS in figure. 2 show that the VBM and CBM states of MoS_2 and CrS_2 monolayers arise mainly from the 4*d* and 3*d* orbitals of the transition metal, respectively. Small contribution from the 3*p* orbitals of the S atoms is noted in both figures. This is in agreement with the results of Dolui *et al*. [55] and Zhuang

Table 1: The theoretical and experimental energy band gaps of the pristine MoS_2 and CrS_2 monolayers.

Structure	Method	Band gap (eV)	Ref.
MoS_2	Experimental	1.9	[51]
	Experimental	1.75	[52]
	GGA	1.67	[49]
	GGA	1.65	This work
	HSE	2.25	[49]
	HSE	2.14	[53]
	HSE	2.17	This work
CrS_2	GGA	0.89	[33]
	GGA	0.86	This work
	HSE	1.48	[54]
	HSE	1.31	This work

et al. [54].

Spin polarized calculations were carried out for all of the calculations in this paper. However, the majority spin DOS are symmetrical to the minority spin DOS, indicating that the systems are non magnetic in nature [33, 56]. Therefore, we only show the DOS for spin-up channel, for the entire paper.

3.2. *Isolated Cr dopants in a MoS_2 monolayer*

Next, we examine the effect of isolated (*I*) one and two Cr dopants on the thermodynamic stability, structural and electronic properties of a MoS_2 monolayer. As mentioned earlier, the Mo and S atoms occupy different sublattices of the hexagonal MoS_2 monolayer as shown in figure. 1.

The Mo atoms occupy one sublattice for the entire structure, and due to the symmetry of the system, we only have one possible unique configuration for single Cr doping shown in figure. 3(a) called $C_{1(I)}$. However, in the case of the two Cr dopants, different configurations are possible.

All the distinct configurations of the two Cr dopants are shown in figure. 3(b)-(e), namely configurations $C_{2(I)}$, $C_{3(I)}$, $C_{4(I)}$ and $C_{5(I)}$. Configuration $C_{2(I)}$ is constructed by introducing the two Cr atoms at the Mo sites within the same hexagonal ring-like in a 5×5 supercell of a MoS_2 monolayer. These

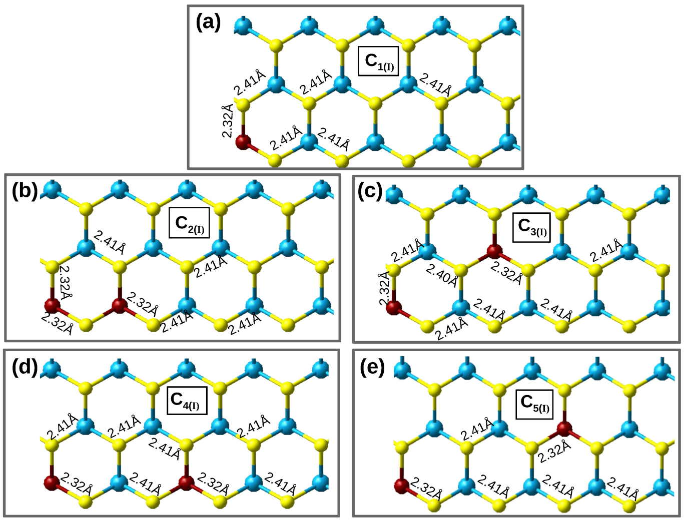

Figure 3: (a) The relaxed structure of a single Cr doping in a MoS_2 monolayer. The various configurations of the two Cr dopants (b) $C_{2(I)}$, (c) $C_{3(I)}$, (d) $C_{4(I)}$ and (e) $C_{5(I)}$. The blue, red and light yellow spheres indicate the Mo, Cr and S atoms, respectively.

two dopants are first nearest neighbor to each other (see figure. 3(b)). The second possible configuration $C_{3(I)}$ involves the second hexagonal ring-like. $C_{3(I)}$ is obtained when the second Cr atom is the second nearest neighbor of the first Cr atom (see figure. 3(c)). Configuration $C_{4(I)}$ is obtained when the second Cr atom is placed as the third nearest neighbor with the first Cr atom (see figure. 3(d)). The last configuration $C_{5(I)}$ is obtained when the second atom is the forth nearest neighbor of the first Cr atom (see figure. 3(e)) considering only the Mo sites.

In order to study the stability of these different configurations, we calculated the formation energies using equation. 2. The formation energy for $C_{1(I)}$ is 2 meV, revealing an endothermic reaction. Figure. 4 summarizes the formation energies for the different configurations of the two dopants in a MoS_2 monolayer ($C_{2(I)}$, $C_{3(I)}$, $C_{4(I)}$ and $C_{5(I)}$). It can be seen that $C_{4(I)}$ has the highest formation energy, while $C_{2(I)}$ possessing the lowest. We realize that the Cr-doped system becomes more unstable when the Cr atoms move farther away from each other. Thus, this is an evidence that the two Cr dopants prefer to be closer to each other in a MoS_2 supercell, when considering the Mo sites only. Although positive, the formation energies shown in figure. 4 are very low, suggesting that Cr-doped configurations can form under reasonable conditions.

In all configurations considered, the Cr-S bond distance is 0.10 Å on average lower than the initial bond length of the MoS_2 monolayer. Various bond lengths can be read from figure. 3. This relatively small value reveals that Cr does not cause significant structural distortions in a MoS_2 monolayer.

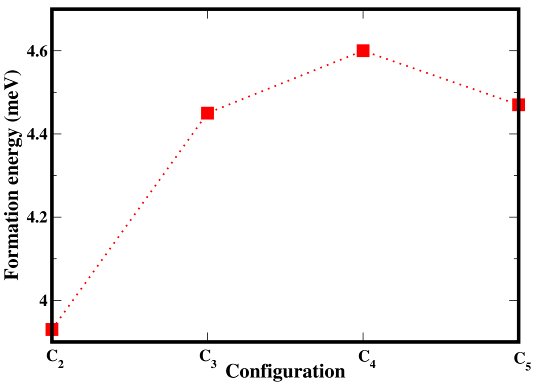

Figure 4: The formation energies for distinct configurations of the two dopants in a MoS_2 monolayer. Along the x axis, configurations $C_{2(I)}$, $C_{3(I)}$, $C_{4(I)}$ and $C_{5(I)}$ denote the first, second, third and forth nearest neighbor Cr atoms.

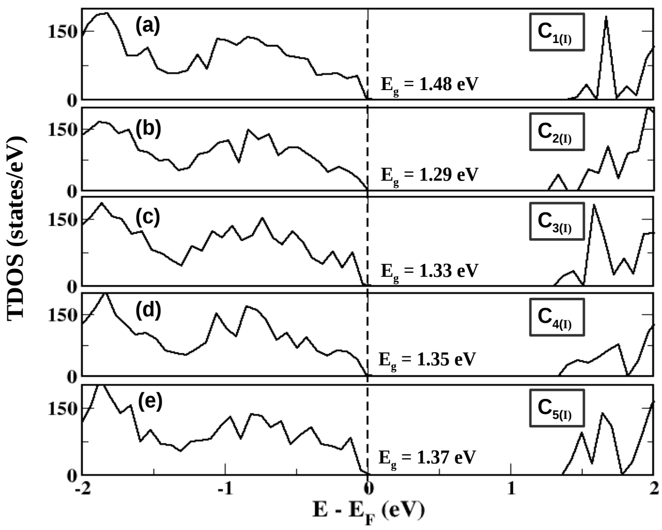

Figure 5: (a) The TDOS of single Cr doping in a MoS_2 monolayer ($C_{1(I)}$). The TDOS of the configurations (b) $C_{2(I)}$, (c) $C_{3(I)}$, (d) $C_{4(I)}$ and (e) $C_{5(I)}$. The black dashed vertical lines indicate the Fermi level.

Figure. 5 presents the TDOS of our distinct Cr configurations in a MoS_2 monolayer. It is found that the incorporation of the Cr dopants preserves the semiconducting properties of

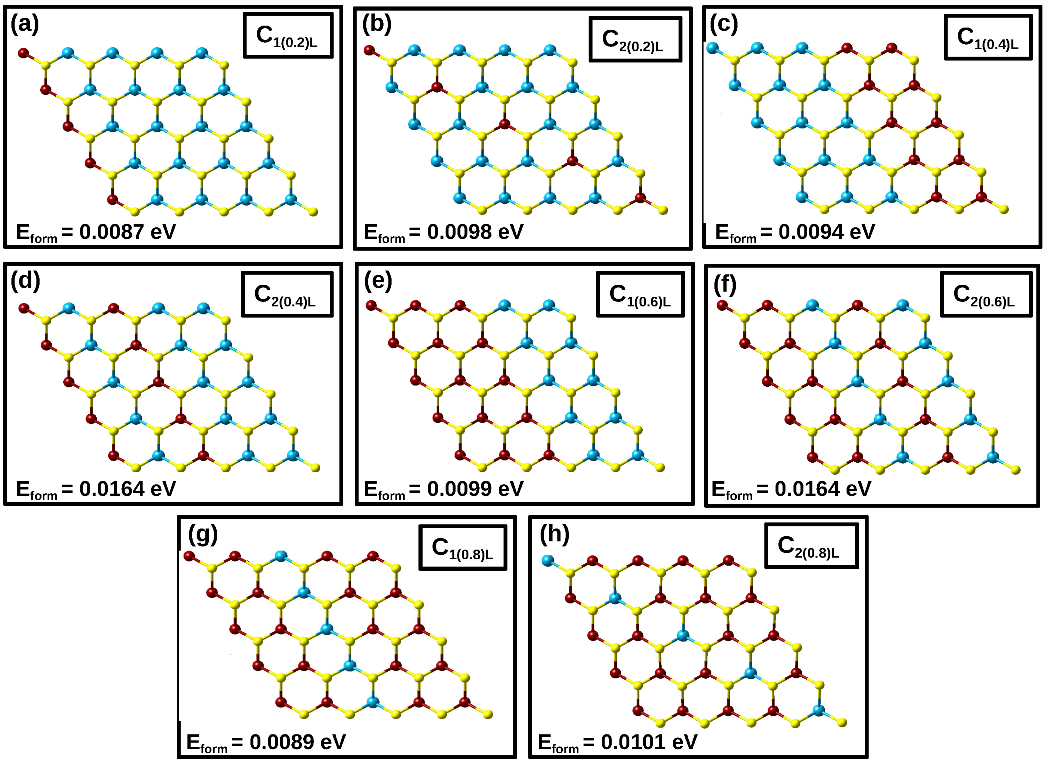

Figure 6: All the possible configurations of line-ordered alloys of $Mo_{1-x}Cr_xS_2$ at each concentration. Configurations (a) $C_{1(0.2)L}$ and (b) $C_{2(0.2)L}$ correspond to 20%, (c) $C_{1(0.4)L}$ and (d) $C_{2(0.4)L}$ to 40%, (e) $C_{1(0.6)L}$ and (f) $C_{2(0.6)L}$ to 60%, and (g) $C_{1(0.8)L}$ and (h) $C_{2(0.8)L}$ to 80% of the Cr atoms. The blue, red and yellow spheres represent the Mo, Cr and S atoms, respectively. The formation energy (E_{form}) of each configuration obtained using equation. 2 is shown at the bottom of each diagram.

MoS_2 monolayer but reduces the band gap of the system significantly. Even at a very low concentration of 4% Cr dopant (one Cr dopant), the band gap has been reduced from 1.65 eV (pristine MoS_2) to 1.48 eV. Comparing different configurations of the two dopants, it is noted that the most stable configuration $C_{2(I)}$ has the smallest band gap (see figure. 5b), while $C_{5(I)}$ possessing the largest (see figure. 5e). Revealing that the band gap can be fine tuned by variation of the distance between the two Cr dopants.

Since these preliminary results suggest that the Cr atoms prefer to be closer to each other, it is important to examine the effect of Cr dopants at high concentrations. In this study, the Cr line-ordered alloy and random alloy at different concentrations and in various configurations are studied. This is further supported by Lewis *et al*. [57] who reported that Cr substituting Mo in a MoS_2 monolayer can be synthesized at high concentration.

3.3. Line-ordered and random alloys of Cr atoms in a MoS_2 monolayer

3.3.1. Thermodynamic stability and structural properties of $Mo_{1-x}Cr_xS_2$ alloys

As mentioned earlier, simulation of the alloys in a layered systems is a great challenge due to thousands of possible atomic arrangements. In this section, a systematic study of Cr line-ordered alloys and random alloys has been considered. Five concentrations ($x = 0.2, x = 0.4, x = 0.6$ and $x = 0.8$ correspond to 20%, 40%, 60%, 80% and 100% Cr atoms) have been chosen.

To create the line-ordered alloys, we substitute the Mo atoms in a MoS_2 monolayer with the Cr atoms at different concentrations, along a particular direction (zigzag and diagonal). At each concentration, distinct configurations are identified and examined. All the possible Cr configurations are shown in fig-

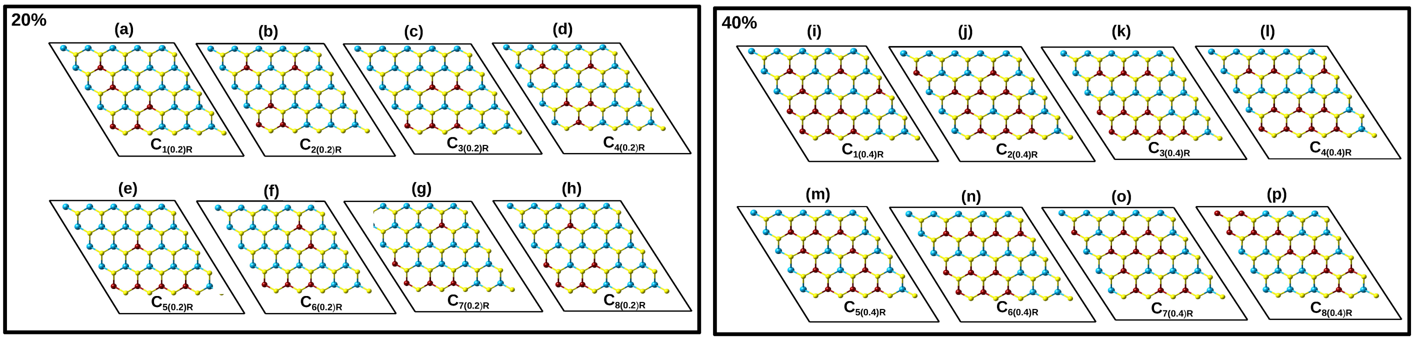

Figure 7: Various selected unique Cr random alloy configurations at 20% of Cr atoms (left panel): (a) $C_{1(0.2)R}$, (b) $C_{2(0.2)R}$, (c) $C_{3(0.2)R}$, (d) $C_{4(0.2)R}$, (e) $C_{5(0.2)R}$, (f) $C_{6(0.2)R}$, (g) $C_{7(0.2)R}$ and (h) $C_{8(0.2)R}$. Those obtained at 40% (right panel) are : (i) $C_{1(0.4)R}$, (j) $C_{2(0.4)R}$, (k) $C_{3(0.4)R}$, (l) $C_{4(0.4)R}$, (m) $C_{5(0.4)R}$, (n) $C_{6(0.4)R}$, (o) $C_{7(0.4)R}$ and (p) $C_{8(0.4)R}$. At 60% and 80% concentrations, the selected configurations are the same as those obtained at 40% and 20%, respectively, but with transition metals swapped. The blue, red and yellow spheres represent the Mo, Cr and S atoms, respectively.

ure. 6 named $C_{1(0.2)L}$, $C_{2(0.2)L}$, $C_{1(0.4)L}$, $C_{2(0.4)L}$, $C_{1(0.6)L}$, $C_{2(0.6)L}$, $C_{1(0.8)L}$ and $C_{1(0.8)L}$. To avoid repetition, the periodic boundary conditions are always taken into account when constructing the line-ordered alloys. Configurations $C_{1(0.2)L}$ and $C_{2(0.2)L}$ correspond to 20% of the Cr atoms. Configuration $C_{1(0.2)L}$ is obtained when the Cr atoms are placed along a zigzag path of the hexagonal MoS_2 monolayer occupying the same Mo sublattice (see figure. 6(a)) and configuration $C_{2(0.2)L}$ is formed by substituting the Mo atoms along the diagonal of the supercell, also occupying the same Mo sites (see figure. 6(b)).

Configurations $C_{1(0.4)L}$ and $C_{2(0.4)L}$ correspond to 40% of the Cr atoms. In $C_{1(0.4)L}$, the Cr atoms constitute two adjacent parallel lines along the zigzag path (see figure. 6(c)). Configuration $C_{2(0.4)L}$ is constructed by two lines of the Cr atoms along the zigzag, but separated by a line of the Mo atoms (see figure. 6(d)). At 40% concentration, the line-ordered alloy along the diagonal is not possible. Following the same pattern, configurations $C_{1(0.6)L}$ and $C_{2(0.6)L}$ are identified in 60% concentration (see figure. 6(e) and figure. 6(f)). Lastly, configurations $C_{1(0.8)L}$ and $C_{2(0.8)L}$ are obtained when 80% of the Cr atoms substitute the Mo atoms. These configurations are similar to those of $C_{1(0.2)L}$ and $C_{2(0.2)L}$ but the transition metal elements are swapped (as shown in figure. 6(g) and figure. 6(h)). It is clear that at each Cr concentration, only two distinct line-ordered alloy configurations are possible.

For random alloys, many unique configurations at each concentration are identified using SQS method. figure. 7 presents the selected unique configurations at 20% and 40% concentrations. For a perfect alloy (optimum pair correlation function of the SQS) at 20% concentration, three Cr-Cr bonds (N_{BB} = 3) should be formed at each configuration as described in the methodology. For instance in configuration $C_{1(0.2)R}$ shown in figure. 7(a), the three Cr atoms adjacent to each other form two Cr-Cr bonds (N_{BB}) and the third Cr-Cr bond is formed relatively far away. In configuration $C_{2(0.2)R}$, three of the introduced Cr atoms substitute the three Mo atoms in the hexagonal ringlike showing a triangular arrangement, forming the required three bonds (figure. 7(b)). The remaining two Cr atoms do not necessarily need to form N_{BB} (Cr-Cr bond). Following the same procedure, configurations $C_{3(0.2)R}$, $C_{4(0.2)R}$, $C_{5(0.2)R}$, $C_{6(0.2)R}$, $C_{7(0.2)R}$ and $C_{8(0.2)R}$ are also identified. The same procedure (SQS model for nearest-neighbor pair) has been applied at 40% concentration. Hence, at 40%, the required N_{BB} = 12 has been met and all the identified configurations are also presented in figure. 7. At 60% and 80% concentrations, all the selected configurations are the same as those obtained at 40% and 20%, respectively, but with transition metals swapped. Some of our configurations are the same as those in ref. [58] for $Mo_{(1-x)}W_xS_2$.

In order to compare the relative stabilities of the Cr line-ordered alloys and random alloys, we have calculated the formation energies using equation. 2. The calculated formation

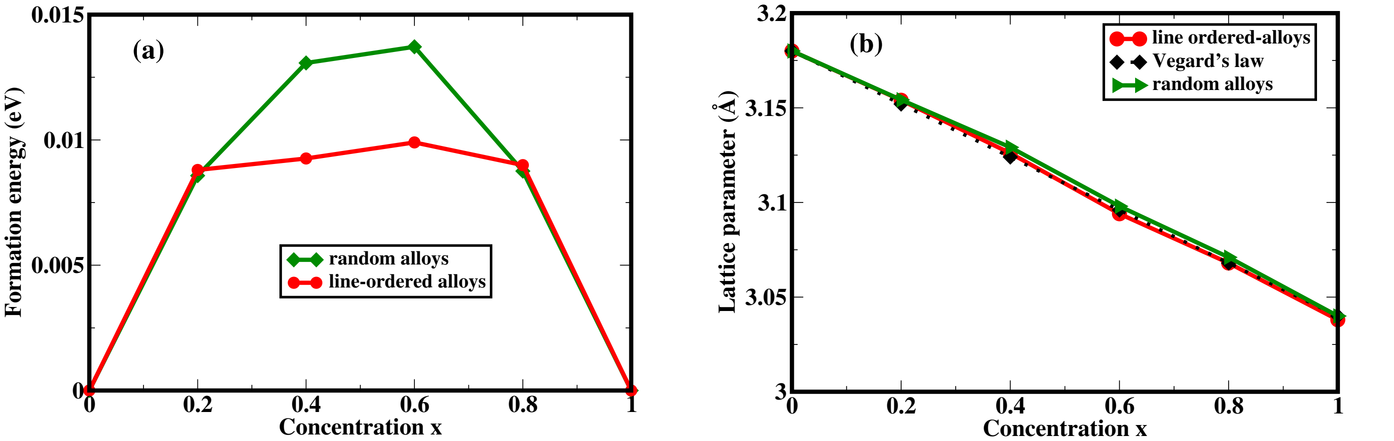

Figure 8: (a) The calculated formation energies of the lowest energy configurations for the Cr line-ordered alloys and random alloys at different concentrations. (b) The lattice constant for $Mo_{1-x}Cr_xS_2$ alloys at different concentrations. The red line connects the lowest energy configurations for the line-ordered alloys while the green line connects those for the Cr random alloys.

energies of the line-ordered alloys are presented in the bottom of each diagram in figure. 6. Although formation of the Cr line-ordered alloys seems to be endothermic (positive formation energy), their magnitude values are relatively very small, suggesting that formation of the Cr alloys in a MoS_2 monolayer can be spontaneous. Comparing the formation energies of the line-ordered alloy configurations at each concentration, we found that $C_{1(0.2)L}$, $C_{1(0.4)L}$, $C_{1(0.6)L}$ and $C_{1(0.8)L}$ are energetically the most stable configurations at 20%, 40%, 60% and 80%, respectively. Configuration $C_{1(0.2)L}$ is 1.1 meV lower than $C_{2(0.2)L}$ in energy at 20% concentration. Since the separations between the Cr atoms are larger in configuration $C_{2(0.2)L}$ than in configuration $C_{1(0.2)L}$, this observation suggests that the interaction of Cr alloys in a MoS_2 monolayer is desirable. Moreover, the major driving force on the stability of these systems is the concentration, because figure. 8(a) shows a parabolic curve revealing that the formation energies of the configurations rise with the increase in Cr or Mo concentration. At 40%, it is noted that configuration $C_{1(0.4)L}$ is more energetically favorable than configuration $C_{2(0.4)L}$. This emphasize an idea that the Cr atoms prefer to be grouped together. It can be seen that when the two Cr lines alloys are separated by a line of the Mo atoms (see figure. 6(d)), the relative stability of configuration $C_{1(0.4)L}$ reduces significantly. This trend is also noted in 60% of the Cr atoms. In configuration $C_{1(0.6)L}$, three Cr lines alloy are grouped together (see figure. 6(e)) but in configuration $C_{2(0.6)L}$, three Cr lines alloy are separated by a line of the Mo atoms (see figure. 6(f)). We observe that configuration $C_{1(0.6)L}$ is more energetically favorable than configuration $C_{2(0.6)L}$. At 80% concentration, we note the same behavior as that of 20%. This is not surprising because in 80% concentration, the Cr atoms occupy the sites of Mo in 20%.

Table. 2 presents the stability of the various Cr random alloy configurations. Just like in the line-ordered alloys, the formation energies of all configurations are positive. Although positive formation energies indicate that $Mo_{1-x}Cr_xS_2$ would prefer

Table 2: Formation energies of the selected unique Cr random alloy configurations at different concentrations x. The bold values represent the lowest energy configurations at each concentration.

	Formation energies (eV)			
Conf.	x = 0.2	x = 0.4	x = 0.6	x = 0.8
C_{1R}	**0.0086**	0.0139	0.0149	**0.0090**
C_{2R}	0.0104	0.0181	0.0169	0.0997
C_{3R}	0.0089	0.0149	0.0147	0.0122
C_{4R}	0.0103	0.0144	0.0146	0.0119
C_{5R}	0.0102	0.0185	0.0179	0.0124
C_{6R}	0.0095	**0.0130**	**0.0145**	0.0095
C_{7R}	0.0097	0.0182	0.0169	0.0091
C_{8R}	0.0100	0.0167	0.0161	0.0124

segregation at 0K [33], their magnitudes are very small suggesting that they can form at temperatures of few degrees Celsius. These Cr random alloys are plausible structures and some of these configurations were synthesized at low concentration [57]. The thermodynamic stability of these alloys greatly depends on the Cr pair coordination (Cr-Cr), see the lowest energy configuration $C_{1(0.2)R}$ shown in figure. 7(a). Apart from $C_{1(0.2)R}$ and $C_{3(0.2)R}$, all other configurations have slighty high formation energies since they possess an unpaired Cr atoms. This is in agreement with Wei *et al*. [33] who reported that the long distance neighbors interaction contribute less energy than nearest-neighbor. Following the pair correlation function, the same behavior is noted at 40% concentration. The most energetically favorable configuration at 40% concentration, $C_{6(0.4)R}$ is shown in figure. 7(n). In this configuration, it is noted that all the Cr atoms are paired showing N_{BB} correlation. All the selected configurations at 60% behave as those at 40%. Similar finding is observed also for 20% and 80% concentrations. Configurations $C_{6(0.6)R}$ and $C_{1(0.8)R}$ to be the most stable at 60% and 80% reveal that even Mo alloys in CrS_2 monolayer would prefer pair coordination.

The formation energies of the most stable structures at each concentration for the two types of alloys considered are plotted in figure. 8(a). We found that at $x = 0.2$ and $x = 0.8$, the energy difference between the Cr line-ordered alloys and Cr random alloys are very small. This might originates from the fact that in both configurations $C_{1(0.2)L}$ and $C_{1(0.2)R}$, the Cr atoms are completely paired to each other enhancing the stability. However, at $x = 0.4$ and $x = 0.6$, the line-ordered alloys have significant lower formation energy than the random alloys. The most stable configurations for the Cr line-ordered alloys $C_{1(0.4)L}$ and $C_{1(0.6)L}$ present a continuous Cr atom pair coordination, whereas in the Cr random alloy configurations ($C_{6(0.4)R}$ and $C_{6(0.6)R}$), there is a Mo line separating the group of paired Cr atoms compromising the stability. Therefore, our results reveal that the line-ordered alloys are plausible structures and can be synthesized at the same conditions as random alloy structures.

We now study the effect of the Cr line-ordered alloys and random alloys on the structural properties of a MoS_2 monolayer. After full relaxation, we note that the incorporation of the Cr atoms into MoS_2 monolayer preserves the hexagonal symmetry of the system but the area changes due to the change in lattice constants. Figure. 8(b) shows how lattice constants of $Mo_{1-x}Cr_xS_2$ alloys change as a function of Cr concentration. We find that the values of the lattice constants for the alloys range between those of pristine MoS_2 and CrS_2 monolayers in both cases. It is also noted in figure. 8(b) that the lattice constants of the configurations are inversely proportional to the Cr concentration. This reduction is specifically due to the smaller atomic radius of Cr atom compared to that of Mo atom. The atomic radii of Cr and Mo are 166 picometers and 190 picometers, respectively [59].

Usually, the physical properties (e.g. lattice constant and band gap) of an alloy $Mo_{1-x}Cr_xS_2$ as a function of the dopants concentration x are described by the following quadratic equation [25, 31, 60]:

$$P(x) = (1 - x)P(MoS_2) + xP(CrS_2) - bx(1 - x)\ , \qquad (6)$$

where $P(MoS_2)$ and $P(CrS_2)$ are the physical properties of the pristine MoS_2 and CrS_2 monolayers, respectively and b is called bowing parameter. It characterizes the degree of deviation from linearity trend.

If b in equation. 6 is equal to zero, the so called Vergard's law is obeyed. This law states that there is a linear relationship between the physical properties of a host material and the concentration of alloys [61, 31]. Then equation. 6 reduces to:

$$P(x) = xP(NX_2) + (1 - x)P(MX_2)\ . \qquad (7)$$

We plotted in figure. 8(b) the lattice constants of the lowest energy configurations for the line-ordered alloys and random alloys as a function of Cr concentration. For comparison purpose, we have plotted also in figure. 8(b), the lattice constants of the alloys using equation. 7. We note that the three plots, for the random and line-ordered alloys and equation. 7, are superimposed on top of each other. It can also be seen in figure. 8(b)

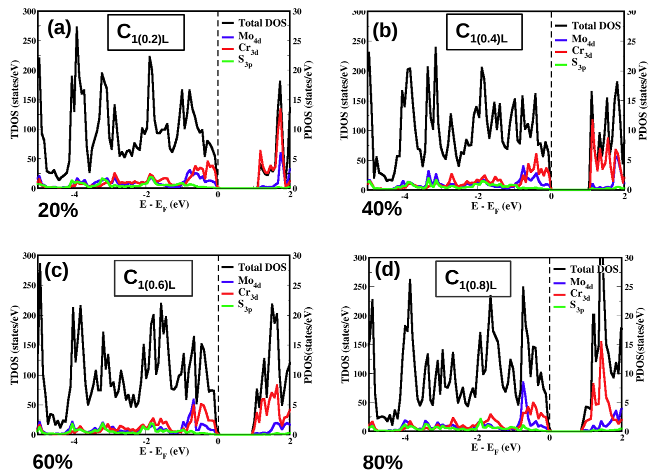

Figure 9: TDOS and PDOS of the stable structures for the Cr line-ordered alloys in a MoS_2 monolayer: (a) $C_{1(0.2)L}$, (b) $C_{1(0.4)L}$, (c) $C_{1(0.6)L}$ and (d) $C_{1(0.8)L}$. The black dashed vertical lines indicate the Fermi level.

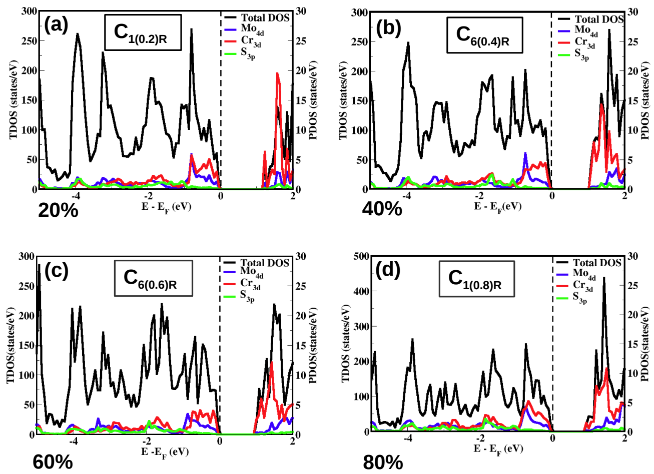

Figure 10: TDOS and PDOS of the stable structures for the Cr random alloys in a MoS_2 monolayer: (a) $C_{1(0.2)R}$, (b) $C_{6(0.4)R}$, (c) $C_{6(0.6)R}$ and (d) $C_{1(0.8)R}$. The black dashed vertical lines indicate the Fermi level.

that the lattice parameters change almost linearly with the Cr concentration. This characteristic of the line-ordered and random alloys obeys Vergard's law.

3.3.2. *Electronic properties of $Mo_{1-x}Cr_xS_2$ alloys*

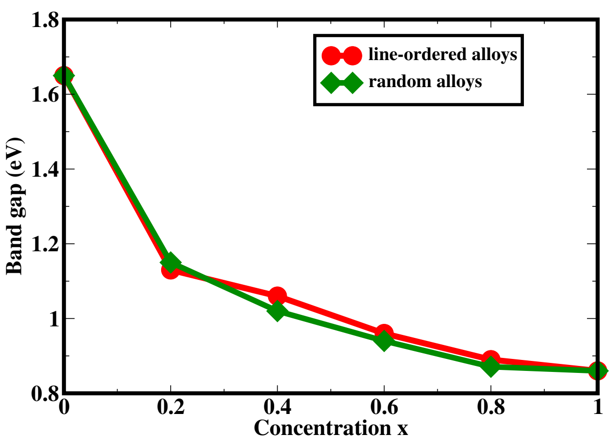

Figure 11: The band gaps of $Mo_{1-x}Cr_xS_2$ line-ordered alloys and random alloys as a function of Cr concentration. Red line connects the band gaps of the most energetically favorable configurations for the line-ordered alloys at each concentration $C_{1(0.2)L}$, $C_{1(0.4)L}$, $C_{1(0.6)L}$ and $C_{1(0.8)L}$, while the green line connects those for the random alloys $C_{1(0.2)R}$, $C_{6(0.4)R}$, $C_{6(0.6)R}$ and $C_{1(0.8)R}$.

To examine the electronic properties of the $Mo_{1-x}Cr_xS_2$ alloys, DOS calculations were carried out. Figure. 9 and figure. 10 show the TDOS and PDOS of the stable structures at 20%, 40%, 60% and 80% of the Cr atoms for the line-ordered alloys and random alloys, respectively.

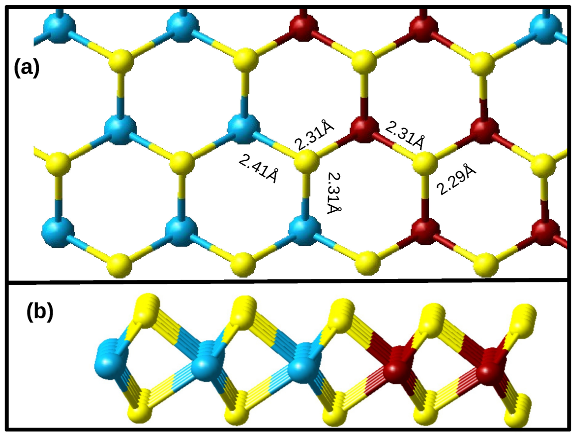

Figure 12: (a)Top view of $Mo_{1-x}Cr_xS_2$ line-ordered alloys showing the deviation in bond lengths due to Cr atoms. (b) Side view of the same $Mo_{1-x}Cr_xS_2$ structure. The blue, red and yellow spheres indicate the Mo, Cr and S atoms, respectively.

We find that these two types of alloys significantly fine tune the band gap of a MoS_2 monolayer. For all Cr concentrations considered, the semiconducting behavior of a MoS_2 monolayer is preserved but the band gap is reduced. Figure. 11 presents the band gap values of the $Mo_{1-x}Cr_xS_2$ alloys calculated at different Cr concentrations. We find that the band gap decreases when the Cr concentration increases. The reason might be due

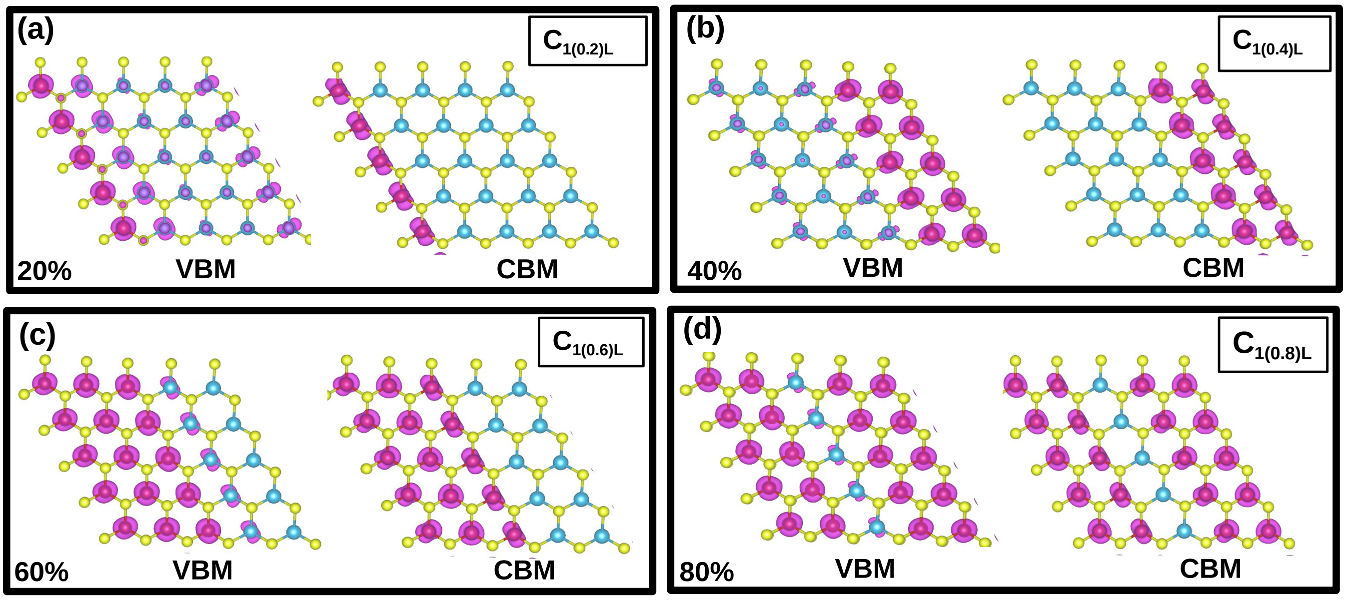

Figure 13: Partial charge densities of the VBM and CBM for the lowest energy line-ordered alloy configurations at (a) 20%, (b) 40%, (c) 60% and (d) 80% Cr concentrations.

to the inward strain along the xy-plane induced by small atomic radii of the Cr atoms compared to those of Mo atoms. No Cr buckling is noted along the z-axis of the MoS_2 monolayer (see figure. 12(b)). Bond lengths of the line-ordered alloys are displayed in figure. 12(a) . The relaxed Cr-S bond length is about 2.31 Å on average (same for both line-ordered alloys and random alloys). This value is 0.1 Å less than that of Mo-S of about 2.41 Å. The deviation in bond lengths should be responsible for reduction of the MoS_2 monolayer band gap as well as the lattice constant. This is opposite to the previous result on isovalent substitution $Mo_xW_{1-x}S_2$, where the band gap increases with the concentration of W atoms [28]. The band gap of $Mo_{1-x}Cr_xS_2$ line-ordered alloys as well as random alloys range between 1.65 ($x = 0$) and 0.86 eV ($x = 1$). This range of band gap is suitable for solar spectrum and thus tuning the band gap of a MoS_2 monolayer has an important role in the solar energy conversion [53]. These values might improve when using other exchange-correlation functionals such as HSE or Green's function (GW) [62].

Subsequently, in order to study the contribution of the Cr orbital states on the reduction of band gap, we analyze the PDOS for stable configurations at 20%, 40%, 60% and 80% shown in figure. 9 and figure. 10. This is to examine if there is any hybridization of Cr, Mo and S orbitals. For all cases, it is noted that the 4d orbitals of the Mo atoms and 3d orbitals of the Cr atoms are the major contributors for the VBM. The 3p orbitals of the S atoms also contribute for the VBM but in a small magnitude. We also find that CBM state is mainly contributed by the 3d orbitals of the Cr atoms. These Cr 3d orbitals states get more populated at the band edges when the Cr concentration increases, thus reducing the band gap significantly as shown in figure. 9(d) and figure. 10(d). We further analyze the partial charge density distribution for VBM and CBM states for the lowest energy line-ordered alloy configurations shown in figure. 13. It is noted indeed that the VBM state is mainly dominated by Mo and Cr charge densities (see figure. 13(a)). The small cloud of charge on the S atoms next to Cr atoms is also noted. On the other hand, the CBM state only arises from the Cr atoms charge density at each concentration. These partial charge densities results confirm the PDOS analysis.

The GGA exchange correlation is known to severely underestimate the band gap of a real material. In order to check the reliability of our previous GGA calculations, we have calculated the TDOS using HSE functional. For the pristine MoS_2 and CrS_2 monolayers, our HSE band gaps are 2.17 eV and 1.31 eV. Our results are in agreement with the previously reported HSE values (as shown in Table. 1). Compared to the experimental data, HSE overestimates the band gap of MoS_2 monolayer ($\sim$+0.25 eV). Due to the high computational cost consuming of the HSE calculations, we calculated the band gaps of lowest energy configurations. At 20% of the Cr atoms, the HSE band gap is 1.62 eV (1.71 eV) for line-ordered (random) alloys more than the GGA value by 0.49 eV (0.64 eV). At 40%, a HSE band gap of 1.53 eV (1.52 eV) has been obtained also more than the GGA predicted value. Although HSE values are more than the GGA values in magnitude, their trends are the same. This suggests that GGA functional can qualitatively describe the line-ordered alloys in a MoS_2 monolayer. Our results suggest that $Mo_{1-x}Cr_xS_2$ line-ordered alloys are essential for nanotechnology devices.

4. Conclusions

In conclusion, using a DFT approach, we have successfully performed a comparative study of the thermodynamic stability, structural and electronic properties of $Mo_{1-x}Cr_xS_2$ line-ordered alloys and random alloys. The lowest energy configuration has been identified at each concentration to predict new plausible materials for nanotechnological device applications. The line-ordered alloys are constantly lower in formation energies than the random alloys at each concentration. Generally, the formation energies for all configurations are found to be very small (close to zero) suggesting that the $Mo_{1-x}Cr_xS_2$ alloys can be synthesized under ambient conditions.

Interestingly, both the line-ordered alloys and random alloys fine tuned the band gap of a MoS_2 monolayer. The Cr concentrations are found to be the major driving force in tuning the band gap of a MoS_2 monolayer. The small atomic radii of the Cr atoms compared to those of Mo atoms induces inward strain in the structure affecting the electronic properties of the MoS_2 monolayer. The hybridization of the Cr 3*d* and Mo 4*d* orbitals occurs at the vicinity of the band edges resulting in the reduction of the band gap. The magnitude of the $Mo_{1-x}Cr_xS_2$ alloys band gap values obtained from GGA and HSE functionals meets the requirements for solar energy conversion and nanotechnological devices applications. The further study of line-ordered alloys is encouraged for other TMD, both theoretically and experimentally.

Acknowledgment

The authors acknowledge the University of Pretoria for financial and computational resources support. REM and NC are also grateful to NRF and NITheP for financial support. We also thank R.C. Andrew and O. Olaniyan for useful discussions.

References

[1] A. K. Geim, K. S. Novoselov, The rise of graphene, Nature materials 6 (3) (2007) 183–191. doi:10.1038/nmat1849.

[2] K. Novoselov, D. Jiang, F. Schedin, T. Booth, V. Khotkevich, S. Morozov, A. Geim, Two-dimensional atomic crystals, Proceedings of the National Academy of Sciences of the United States of America 102 (30) (2005) 10451–10453. doi:10.1073/pnas.0502848102.

[3] H. Zhang, Ultrathin two-dimensional nanomaterials, ACS nano 9 (10) (2015) 9451–9469. doi:10.1021/acsnano.5b05040.

[4] A. C. Neto, F. Guinea, N. M. Peres, K. S. Novoselov, A. K. Geim, The electronic properties of graphene, Reviews of modern physics 81 (1) (2009) 109. doi:10.1103/revmodphys.81.109.

[5] M. Xu, T. Liang, M. Shi, H. Chen, Graphene-like two-dimensional materials, Chemical reviews 113 (5) (2013) 3766–3798. doi:10.1021/cr300263a.

[6] K. S. Novoselov, A. K. Geim, S. V. Morozov, D. Jiang, Y. Zhang, S. V. Dubonos, I. V. Grigorieva, A. A. Firsov, Electric field effect in atomically thin carbon films, science 306 (5696) (2004) 666–669. doi:10.1126/science.1102896.

[7] O. Olaniyan, R. Mapasha, D. Momodu, M. Madito, A. Kahleed, F. Ugbo, A. Bello, F. Barzegar, K. Oyedotun, N. Manyala, Exploring the stability and electronic structure of beryllium and sulphur co-doped graphene: a first principles study, RSC Advances 6 (91) (2016) 88392–88402. doi:10.1039/C6RA17640B.

[8] A. Hussain, S. Ullah, M. A. Farhan, Fine tuning of band-gap of graphene by atomic and molecular doping: A density functional theory study, RSC Advances 6 (61) (2016) 55990–56003. doi:10.1039/c6ra04782c.

[9] P. Rani, V. Jindal, Designing band gap of graphene by B and N dopant atoms, RSC Advances 3 (3) (2013) 802–812. doi:10.1039/c2ra22664b.

[10] J. O. Sofo, A. S. Chaudhari, G. D. Barber, Graphane: a two-dimensional hydrocarbon, Physical Review B 75 (15) (2007) 153401. doi:10.1103/physrevb.75.153401.

[11] X. Gao, Z. Wei, V. Meunier, Y. Sun, S. B. Zhang, Opening a large band gap for graphene by covalent addition, Chemical Physics Letters 555 (2013) 1–6. doi:10.1016/j.cplett.2012.10.069.

[12] D. Pacile, J. Meyer, C. O. Girit, A. Zettl, The two-dimensional phase of boron nitride: few-atomic-layer sheets and suspended membranes, Applied Physics Letters 92 (13) (2008) 133107. doi:10.1063/1.2903702.

[13] Q. H. Wang, K. Kalantar-Zadeh, A. Kis, J. N. Coleman, M. S. Strano, Electronics and optoelectronics of two-dimensional transition metal dichalcogenides, Nature nanotechnology 7 (11) (2012) 699–712. doi:10.1038/nnano.2012.193.

[14] A. Kuc, T. Heine, A. Kis, Electronic properties of transition-metal dichalcogenides, MRS Bulletin 40 (07) (2015) 577–584. doi:10.1557/mrs.2015.143.

[15] B. Radisavljevic, A. Radenovic, J. Brivio, i. V. Giacometti, A. Kis, Single-layer MoS_2 transistors, Nature nanotechnology 6 (3) (2011) 147–150. doi:10.1038/nnano.2010.279.

[16] H. Zeng, J. Dai, W. Yao, D. Xiao, X. Cui, Valley polarization in MoS_2 monolayers by optical pumping, Nature nanotechnology 7 (8) (2012) 490–493. doi:10.1038/nnano.2012.95.

[17] A. Castellanos-Gomez, M. Poot, G. A. Steele, H. S. van der Zant, N. Agraït, G. Rubio-Bollinger, Elastic properties of freely suspended MoS_2 nanosheets, Advanced Materials 24 (6) (2012) 772–775. doi:10.1002/adma.201103965.

[18] N. izyumskaya, D. O. Demchenko, V. Avrutin, Ü. ÖZGÜR, H. MorkoÇ, Two-dimensional MoS_2 as a new material for electronic devices, Turkish Journal of Physics 38 (3) (2014) 478–496. doi:10.3906/fiz-1407-16.

[19] H. Wang, H. Yuan, S. S. Hong, Y. Li, Y. Cui, Physical and chemical tuning of two-dimensional transition metal dichalcogenides, Chemical Society Reviews 44 (9) (2015) 2664–2680. doi:10.1039/c4cs00287c.

[20] C. Ataca, H. Sahin, S. Ciraci, Stable, single-layer MX_2 transition-metal oxides and dichalcogenides in a honeycomb-like structure, The Journal of Physical Chemistry C 116 (16) (2012) 8983–8999. doi:10.1021/jp212558p.

[21] M. Berger, Nanotechnology: The Future is Tiny, Royal Society of Chemistry, 2016.

[22] X. Li, H. Zhu, Two-dimensional MoS_2: Properties, preparation, and applications, Journal of Materiomics 1 (1) (2015) 33–44. doi:10.1016/j.jmat.2015.03.003.

[23] I. Vurgaftman, J. Meyer, L. Ram-Mohan, Band parameters for III–V compound semiconductors and their alloys, Journal of applied physics 89 (11) (2001) 5815–5875. doi:10.1063/1.1368156.

[24] M. Ameri, A. Bentouaf, M. Doui-Aici, R. Khenata, F. Boufadi, A. Touia, et al., Structural and electronic properties calculations of $Al_xIn_{1-x}P$ alloy, Materials Sciences and Applications 2 (07) (2011) 729–738. doi:10.4236/msa.2011.27101.

[25] S. Kumar, S. Joshi, S. Gupta, S. Auluck, Band gap engineering of $CuAl_{(1-x)}In_xS_2$ alloys for photovoltaic applications: a first principles study, Journal of Physics D: Applied Physics 49 (20) (2016) 205103. doi:10.1088/0022-3727/49/20/205103.

[26] W. Zhang, X. Li, T. Jiang, J. Song, Y. Lin, L. Zhu, X. Xu, CVD synthesis of $Mo_{1-x}W_xS_2$ and $MoS_{2(1-x)}Se_{2x}$ alloy monolayers aimed at tuning the bandgap of molybdenum disulfide, Nanoscale 7 (32) (2015) 13554–13560. doi:10.1039/c5nr02515j.

[27] J. Xi, T. Zhao, D. Wang, Z. Shuai, Tunable electronic properties of two-dimensional transition metal dichalcogenide alloys: a first-principles prediction, The journal of physical chemistry letters 5 (2) (2013) 285–291. doi:10.1021/jz402375s.

[28] H.-P. Komsa, A. V. Krasheninnikov, Two-dimensional transition metal dichalcogenide alloys: stability and electronic properties, The journal of physical chemistry letters 3 (23) (2012) 3652–3656. doi:10.1021/jz301673x.

[29] S. Tongay, D. S. Narang, J. Kang, W. Fan, C. Ko, A. V. Luce, K. X. Wang, J. Suh, K. Patel, V. Pathak, et al., Two-dimensional semiconductor alloys: Monolayer $Mo_{1-x}W_xSe_2$, Applied Physics Letters 104 (1) (2014) 012101. doi:10.1063/1.4834358.

[30] L. Xie, Two-dimensional transition metal dichalcogenide alloys: preparation, characterization and applications, Nanoscale 7 (44) (2015) 18392–18401. doi:10.1039/c5nr05712d.

[31] J. Kang, S. Tongay, J. Li, J. Wu, Monolayer semiconducting transition metal dichalcogenide alloys: Stability and band bowing, Journal of Applied Physics 113 (14) (2013) 143703. doi:10.1063/1.4799126.

[32] L.-Y. Gan, Q. Zhang, Y.-J. Zhao, Y. Cheng, U. Schwingenschlögl, Order-disorder phase transitions in the two-dimensional semiconducting transition metal dichalcogenide alloys $Mo_{1-x}W_xX_2$ (X= S, Se, and Te), Scientific reports 4 (2014) 6691. doi:10.1038/srep06691.

[33] X.-L. Wei, H. Zhang, G.-C. Guo, X.-B. Li, W.-M. Lau, L.-M. Liu, Modulating the atomic and electronic structures through alloying and heterostructure of single-layer MoS_2, Journal of Materials Chemistry A 2 (7) (2014) 2101–2109. doi:10.1039/c3ta13659k.

[34] H.-P. Komsa, S. Kurasch, O. Lehtinen, U. Kaiser, A. V. Krasheninnikov, From point to extended defects in two-dimensional MoS_2: evolution of atomic structure under electron irradiation, Physical Review B 88 (3) (2013) 035301. doi:10.1103/physrevb.88.035301.

[35] A. Zunger, S.-H. Wei, L. Ferreira, J. E. Bernard, Special quasirandom structures, Physical Review Letters 65 (3) (1990) 353. doi:10.1103/physrevlett.65.353.

[36] G. Kresse, J. Hafner, Ab initio molecular dynamics for liquid metals, Physical Review B 47 (1) (1993) 558. doi:10.1103/physrevb.47.558.

[37] G. Kresse, J. Furthmüller, Efficiency of ab-initio total energy calculations for metals and semiconductors using a plane-wave basis set, Computational Materials Science 6 (1) (1996) 15–50. doi:10.1016/

0927-0256(96)00008-0.

[38] P. E. Blöchl, Projector augmented-wave method, Physical Review B 50 (24) (1994) 17953. doi:10.1103/physrevb.50.17953.

[39] J. P. Perdew, K. Burke, M. Ernzerhof, Generalized gradient approximation made simple, Physical review letters 77 (18) (1996) 3865. doi:10.1103/physrevlett.77.3865.

[40] T. L. Tan, M.-F. Ng, G. Eda, Stable monolayer transition metal dichalcogenide ordered alloys with tunable electronic properties, The Journal of Physical Chemistry C 120 (5) (2016) 2501–2508. doi:10.1021/acs.jpcc.5b10739.

[41] A. D. Becke, Density-functional exchange-energy approximation with correct asymptotic behavior, Physical review A 38 (6) (1988) 3098. doi:10.1103/PhysRevA.38.3098.

[42] J. P. Perdew, Density-functional approximation for the correlation energy of the inhomogeneous electron gas, Physical Review B 33 (12) (1986) 8822. doi:10.1103/PhysRevB.33.8822.

[43] C. Lee, W. Yang, R. G. Parr, Development of the colle-salvetti correlation-energy formula into a functional of the electron density, Physical review B 37 (2) (1988) 785. doi:10.1103/PhysRevB.37.785.

[44] J. P. Perdew, A. Ruzsinszky, G. I. Csonka, O. A. Vydrov, G. E. Scuseria, L. A. Constantin, X. Zhou, K. Burke, Restoring the density-gradient expansion for exchange in solids and surfaces, Physical Review Letters 100 (13) (2008) 136406. doi:10.1103/PhysRevLett.100.136406.

[45] J. Heyd, G. E. Scuseria, M. Ernzerhof, Hybrid functionals based on a screened coulomb potential, The Journal of Chemical Physics 118 (18) (2003) 8207–8215. doi:10.1063/1.1564060.

[46] C. Jiang, C. Wolverton, J. Sofo, L.-Q. Chen, Z.-K. Liu, First-principles study of binary bcc alloys using special quasirandom structures, Physical Review B 69 (21) (2004) 214202. doi:10.1103/physrevb.69.214202.

[47] X.-L. Fan, Y. Yang, P. Xiao, W.-M. Lau, Site-specific catalytic activity in exfoliated MoS_2 single-layer polytypes for hydrogen evolution: basal plane and edges, Journal of Materials Chemistry A 2 (48) (2014) 20545–20551. doi:10.1039/c4ta05257a.

[48] D. Yang, S. J. Sandoval, W. Divigalpitiya, J. Irwin, R. Frindt, Structure of single-molecular-layer MoS_2, Physical Review B 43 (14) (1991) 12053. doi:10.1103/physrevb.43.12053.

[49] Y. Ding, Y. Wang, J. Ni, L. Shi, S. Shi, W. Tang, First principles study of structural, vibrational and electronic properties of graphene-like MX_2 (M= Mo, Nb, W, Ta; X= S, Se, Te) monolayers, Physica B: Condensed Matter 406 (11) (2011) 2254–2260. doi:10.1016/j.physb.2011.03.044.

[50] H. Guo, N. Lu, L. Wang, X. Wu, X. C. Zeng, Tuning electronic and magnetic properties of early transition-metal dichalcogenides via tensile strain, The Journal of Physical Chemistry C 118 (13) (2014) 7242–7249. doi:10.1021/jp501734s.

[51] K. F. Mak, C. Lee, J. Hone, J. Shan, T. F. Heinz, Atomically thin MoS_2: a new direct-gap semiconductor, Physical Review Letters 105 (13) (2010) 136805. doi:10.1103/physrevlett.105.136805.

[52] A. Splendiani, L. Sun, Y. Zhang, T. Li, J. Kim, C.-Y. Chim, G. Galli, F. Wang, Emerging photoluminescence in monolayer MoS_2, Nano letters 10 (4) (2010) 1271–1275. doi:10.1021/nl903868w.

[53] M. Faraji, M. Sabzali, S. Yousefzadeh, N. Sarikhani, A. Ziashahabi, M. Zirak, A. Moshfegh, Band engineering and charge separation in the $Mo_{1-x}W_xS_2/TiO_2$ heterostructure by alloying: first principle prediction, RSC Advances 5 (36) (2015) 28460–28466. doi:10.1039/c5ra00330j.

[54] H. L. Zhuang, M. D. Johannes, M. N. Blonsky, R. G. Hennig, Computational prediction and characterization of single-layer CrS_2, Applied Physics Letters 104 (2) (2014) 022116. doi:10.1063/1.4861659.

[55] K. Dolui, I. Rungger, C. D. Pemmaraju, S. Sanvito, Possible doping strategies for MoS_2 monolayers: An ab initio study, Physical Review B 88 (7) (2013) 075420. doi:10.1103/physrevb.88.075420.

[56] W. S. Yun, J. Lee, Unexpected strong magnetism of cu doped single-layerMoS_2 and its origin, Physical Chemistry Chemical Physics 16 (19) (2014) 8990–8996. doi:10.1039/c4cp00247d.

[57] D. J. Lewis, A. A. Tedstone, X. L. Zhong, E. A. Lewis, A. Rooney, N. Savjani, J. R. Brent, S. J. Haigh, M. G. Burke, C. A. Muryn, et al., Thin films of molybdenum disulfide doped with chromium by aerosol-assisted chemical vapor deposition (AACVD), Chemistry of Materials 27 (4) (2015) 1367–1374. doi:10.1021/cm504532w.

[58] Y. Chen, J. Xi, D. O. Dumcenco, Z. Liu, K. Suenaga, D. Wang, Z. Shuai, Y.-S. Huang, L. Xie, Tunable band gap photoluminescence from atomically thin transition-metal dichalcogenide alloys, Acs Nano 7 (5) (2013) 4610–4616. doi:10.1021/nn401420h.

[59] E. Clementi, D. Raimondi, W. Reinhardt, Atomic screening constants from scf functions. II. atoms with 37 to 86 electrons, The Journal of chemical physics 47 (4) (1967) 1300–1307. doi:10.1063/1.1712084.

[60] Y. Huang, X. Chen, D. Zhou, H. Liu, C. Wang, J. Du, L. Ning, S. Wang, Stabilities, electronic and optical properties of $SnSe_{2(1-x)}S_{2x}$ alloys: A first-principles study, The Journal of Physical Chemistry C 120 (10) (2016) 5839–5847. doi:10.1021/acs.jpcc.6b00794.

[61] A. R. Denton, N. W. Ashcroft, Vegards law, Physical review A 43 (6) (1991) 3161. doi:10.1103/physreva.43.3161.

[62] P. Rinke, A. Qteish, J. Neugebauer, C. Freysoldt, M. Scheffler, Combining GW calculations with exact-exchange density-functional theory: an analysis of valence-band photoemission for compound semiconductors, New Journal of Physics 7 (1) (2005) 126. doi:10.1088/1367-2630/7/1/126.